Effects of different geomagnetic storm drivers on the ring current: CRCM results

W. D. Cramer,[1] N. E. Turner,[1] M.-C. Fok,[2] and N. Y. Buzulukova[3,4]

Received 21 September 2012; revised 14 January 2013; accepted 16 January 2013; published 4 March 2013.

[1] The storm-time magnetic disturbance at the Earth's equator, as commonly measured by the *Dst* index, is induced by currents in the near-Earth magnetosphere. The ring current is generally considered the most important contributor, but other magnetospheric currents have also been found to have significant effects. Of the two main types of solar geomagnetic storm drivers, Coronal Mass Ejections (CMEs) tend to have a much greater impact on *Dst* than Corotating Interaction Regions (CIRs). Ring current models have been found to underestimate *Dst*, particularly during storms driven by CIRs. One possible explanation is that the models neglect to handle some aspect of ring current physics that is particularly important for CIRs. This study uses the Comprehensive Ring Current Model (CRCM) to estimate the ring current contribution to *Dst* for a selection of storms of various strengths and different drivers (CMEs and CIRs) that have solar wind parameters that fit a typical profile. The model boundary is set to 10 R_E at the equator, encompassing the entire ring current region. The magnetic field is held fixed, based on average storm parameters, which limits our model results to the effects of convection and plasma sheet density at the model boundary. Our model results generally show good agreement with the size and timing of fluctuations in *Dst*, which indicates that convection and boundary conditions play an important role in shaping *Dst*. We also find excellent agreement with the magnitude of *Dst* for CME-driven storms. For CIR-driven storms, however, the magnitude at the peak of the storm frequently deviates from actual *Dst*. In general, we agree with the results of previous research that CIR-driven storms are more underpredicted. However, this study includes some weaker CIR-driven storms for which *Dst* is actually overpredicted. Overall, when examining the dependence of modeled *Dst** on actual *Dst** at storm peak, we find that there is a statistically significant difference between CME- and CIR-driven storms. We also find that approximately half of the total ring current energy lies beyond an L-value of 6.6. However, this figure could be overestimated due to the use of a static magnetic field, which limits radial transport.

Citation: Cramer, W. D., N. E. Turner, M.-C. Fok, and N. Y. Buzulukova (2013), Effects of different geomagnetic storm drivers on the ring current: CRCM results, *J. Geophys. Res. Space Physics*, *118*, 1062–1073, doi:10.1002/jgra.50138.

1. Introduction

1.1. Storm-Time Magnetic Disturbance

[2] Geomagnetic storms are defined by periods of disturbed surface magnetic field at the Earth's equator. This disturbance is typically measured by the *Dst* index, and is primarily caused by the ring current [*Turner et al.*, 2001]. The *Dst* index has some known biases, however, largely due to the geographic location of the magnetometer stations whose measurements are used in its derivation [*Häkkinen et al.*, 2003]. Additionally, other magnetospheric current systems, such as field-aligned currents, ionospheric currents, and the tail current, exert a significant influence [*Campbell*, 1996]. The tail current is the most fractionally significant of these currents, as it has been found to contribute approximately 20–25% of the total value [*Turner et al.*, 2000, 2002; *Ohtani et al.*, 2001]). Ground currents induced by magnetospheric currents also contribute to the surface magnetic disturbance. They have been estimated to increase the total disturbance by around 25% [*Langel and Estes*, 1985; *Häkkinen et al.*, 2002], meaning that they constitute approximately 20% of the measured *Dst*.

[3] The *Dst** index, originally developed by *Burton et al.* [1975], represents the total equatorial field at the Earth's

[1]Department of Physics and Space Sciences, Florida Institute of Technology, Melbourne, Florida, USA.
[2]NASA Goddard Space Flight Center, Greenbelt, Maryland, USA.
[3]CRESST and Geospace Physics Laboratory, NASA Goddard Space Flight Center, Greenbelt, Maryland, USA.
[4]Department of Astronomy, University of Maryland, College Park, Maryland, USA.

Corresponding author: W. D. Cramer, Department of Physics and Space Sciences, Florida Institute of Technology, 150 W. University Ave., Melbourne, FL 32901, USA. (wcramer@my.fit.edu)

©2013. American Geophysical Union. All Rights Reserved.
2169-9380/13/10.1002/jgra.50138

surface produced by all magnetospheric current systems except solar wind pressure-induced currents. Unlike *Dst*, it includes the effects of quiet-time currents. An additional correction for ground-induced currents is also commonly included, as shown in Equation (1).

$$Dst^* \equiv \frac{Dst - b\sqrt{P_{\mathrm{dyn}}} + c}{a} \text{ [nT]} \tag{1}$$

[4] In this equation, P_{dyn} represents the solar wind dynamic pressure in *nPa*, *c* represents the quiet-time current contribution, and *a* represents the ground current correction factor. Various values of constants *a*, *b*, and *c* have been determined by *Burton et al*. [1975], *O'Brien and McPherron* [2000], *Fenrich and Luhmann* [1998], and others.

1.2. Ring Current Energy Gain and Loss Processes

[5] Plasma sheet density and convection strength have been found to be the two primary drivers for ring current strength [*Kozyra and Liemohn*, 2003]. When the interplanetary magnetic field (IMF) has a southward component in the frame of the Earth's magnetic field, solar wind energy can couple into the magnetosphere through magnetic reconnection with the Earth's magnetic field. The resulting convection strengthens the electric field in the magnetotail, which transports plasma sheet particles to the inner magnetosphere through $\vec{E} \times \vec{B}$ drift while also energizing them [*Ganushkina et al*., 2000]. *Fritz* [2001] offered an alternative explanation, suggesting that particle entry and acceleration may take place in the magnetospheric cusp. Sub-storms have been shown to energize the ring current directly through impulsive electric fields [*Baker and Daglis*, 2006] and non-adiabatic acceleration of O^+ during dipolarization [*Fok et al*., 2006], as well as indirectly though increased ionospheric outflow to the plasma sheet [*Daglis*, 2006]. In addition, radial diffusion has been found to contribute significantly to the higher energy population as a result of fluctuating fields during a storm's main phase [*Lyons and Schulz*, 1989], particularly during a storm with a long main phase [*Fok et al*., 1996].

[6] Ring current energy density is lost through a variety of processes. In the early part of the storm when convection is strongest, newly injected particles can escape the region on open drift paths. When convection weakens, the region of closed drift paths expands, trapping near-Earth particles. At this point, charge exchange collisions with neutral exospheric particles become the dominant energy loss process [*Kozyra and Liemohn*, 2003]. Coulomb collisions with plasmaspheric electrons also remove energy from the ring current but are significant only for lower energies [*Fok et al*., 1991]. Particles are also lost through pitch angle diffusion into the atmosphere by electromagnetic waves in the plasmasphere, primarily near the plasmapause [*Fok et al*., 2005; *Jordanova et al*., 1996; *Jordanova et al*., 1997].

1.3. Effects of Different Storm Drivers

[7] Geomagnetic storms are caused by a variety of solar wind disturbances, the most common of which are Coronal Mass Ejections (CMEs) and Corotating Interaction Regions (CIRs). CMEs are collections of relatively dense material that are ejected from the Sun. They are the most common instigator of storm behavior and can be extremely disruptive to the magnetosphere. CMEs frequently cause prolonged periods of steady, disturbed interplanetary magnetic field (IMF) [e.g., *Turner et al*., 2009]. When the IMF is directed southward (i.e., B_z is negative), solar wind energy is deposited into the magnetosphere through magnetic reconnection between the IMF and Earth's magnetic field [*Dungey*, 1961]. CIRs are compressed regions caused by the interaction of slow and fast solar wind. Fast solar wind is usually caused by a high-speed stream (HSS) which emanates from a region of open field lines on the Sun called a coronal hole. When the fast wind impinges on the leading slow solar wind, it creates a compressed region [*Denton and Borovsky*, 2009]. The large-amplitude Alfvén waves associated with high-speed streams cause fluctuating periods of southward IMF B_z that deposit energy into the magnetosphere and drive sustained auroral electrojet activity [*Burke et al*., 2010; *Tsurutani and Gonzalez*, 1987]. CIR-driven storms are generally weaker than those driven by CMEs, rarely resulting in $Dst < -160$ nT. Some researchers have studied the overall energy deposition into the magnetosphere-ionosphere system during all types of magnetic disturbances [*Turner*, 2000; *Baker et al*., 2001; *Pulkkinen et al*., 2002, 1997], but when studies are focused on CIR- and CME-driven events, CIRs have been found to deposit solar wind energy more efficiently into the magnetosphere [*Turner et al*., 2006, 2009].

[8] Few studies using spacecraft data have been done looking at the role of the ring current in CIR-driven events. One study conducted using POLAR data focused on solar minimum conditions in general [*Pulkkinen et al*., 2001]. Ring current models (such as those employed by *Liemohn and Jazowski* [2008], *Jordanova et al*. [1997], *Chen et al*. [1997], and [*Fok et al*., 2001]) can be used to estimate the surface magnetic disturbance using the calculated ring current energy. A few studies have found models to be generally worse at reproducing *Dst* during storms driven by CIRs. Both *Jordanova* [2006] and *Jordanova et al*. [2009] used the RAM model to reproduce the ring current during a CME-driven storm and a CIR-driven storm of similar strength. In both studies, researchers found that *Dst* during the CME more closely followed model predictions than the CIR. They suggested that additional injections into the inner magnetosphere by radial diffusion or sub-storms during CIR-driven storms could explain the difference. *Liemohn et al*. [2010] found that HEIDI model estimates of *Dst** at storm peak for CIR-driven storms were underestimated by 20–30% more than CME-driven storms. They proposed that currents external to the ring current, particularly the tail current, were the most likely cause of this discrepancy because indications are that these currents are stronger and contribute more to *Dst* during CIR-driven storms. Coupling that with the finding of *Ganushkina et al*. [2004] that the tail current is the primary contributor to *Dst* for storms with minimum $Dst > -150$ nT, they reason that the additional tail current contribution could make up the difference seen in their results. In a followup study, *Liemohn and Katus* [2012] compared model estimates of *Dst** with actual *Dst** for a 72 h period surrounding storm peak and concluded that there is a fundamental difference between the inner magnetosphere responses for the two driver types.

[9] This study uses the Comprehensive Ring Current Model (CRCM) to investigate the cause of the evident

dependence of model-derived *Dst** on storm driver. Twenty-four CME- and CIR-driven storms of various strengths, whose IMF B_z and solar wind velocity and density best matched typical profiles, are modeled by the CRCM to reproduce the total ring current energy as a function of storm time. These energy values are used to estimate the *Dst** at the storm peak (as determined by the time of minimum *Dst**), which is compared to actual *Dst**. These results are then compared to previous studies and used to determine if any driver dependence actually exists.

2. Methodology

2.1. Data Sources

[10] The data sets used in this study are provided by OMNIWeb (IMF, solar wind velocity and density), the Kyoto World Data Center (Ap, Kp, AE, and *Dst*), and the NOAA NGDC (F10.7 flux). OMNIWeb solar wind data are provided already time shifted to Earth from the location of the source spacecraft (IMP-8, Geotail, ACE, or Wind). Hourly data sets were obtained from CDAWeb (http://cdaweb.gsfc.nasa.gov/), while higher frequency data were obtained from the original source websites.

2.2. Estimating the Magnetic Disturbance

[11] *Dst**, as defined by equation (1), is used to estimate the surface magnetic disturbance due to all magnetospheric current systems except those caused by solar wind pressure. This study uses the values of constants *b* and *c* derived by *Fenrich and Luhmann* [1998] (15.8 and 20, respectively). The effects of ground-induced currents are removed by setting *a* to 1.25.

[12] The theoretical field produced by the total CRCM ring current energy content, hereafter referred to as ΔB, is calculated using the Dessler-Parker-Sckopke (DPS) relation [*Dessler and Parker*, 1959; *Sckopke*, 1966]. When a dipole magnetic field is assumed, the DPS relation becomes approximately represented by (2), where ΔB is in nT and W_{RC} is the total ring current energy in *keV* (similar to *Liemohn and Jazowski* [2008]).

$$\Delta B = -4.0 \cdot 10^{-30} W_{RC} \text{ [nT]} \tag{2}$$

2.3. Storm Selection

[13] The storms used in this study are taken from a database of storms identified by *Dst** excursions below –50 nT (using constants from *O'Brien and McPherron* [2000] in Equation (1) without the ground-induced current correction) in the period of 1995 to 2006. This cutoff is selected to isolate actual event-driven storms from periods of transient storm-like solar wind conditions. The driver for each storm is identified by referencing *Zhang et al*. [2007a], *Zhang et al*. [2007b], *Cane and Richardson* [2003] (with additional personal communication from the authors), and the weekly Preliminary Report and Forecast of Solar Geophysical Data published by NOAA since 1997. No distinction is made between the different classifications of CMEs (magnetic cloud events, etc.). Storms with data gaps larger than 30 min prior to the storm peak are eliminated from consideration to prevent divergence of model and actual magnetospheric response, except in a few cases where the solar wind and IMF appear to be steady. Only storms with quiet solar wind conditions (steady, low absolute *Dst*) during the 12 h immediately prior to storm onset are considered.

[14] To account for the wide variation in storm solar wind profiles, preference is given to the storms whose associated solar wind inputs best match a typical profile for storms with the same driver. Figure 1 shows the CME and CIR solar wind (velocity and density) and IMF (magnetic field *z* component) profiles used for this study. The values are derived from a superposed epoch analysis of solar wind conditions during storms with a minimum *Dst** $\geq$ –120 nT. There are some clear differences between solar wind conditions for the different drivers. For CMEs, the north-south component of the IMF is more northward (positive B_z) in early recovery than for CIRs. The solar wind velocity is higher for CIRs during storm-time, except for very early in the storm.

[15] A variety of storm strengths (based on minimum *Dst**) is used to smoothly cover the range from weak to strong (minimum *Dst** of –126 nT and –366 nT for CIRs and CMEs, respectively). Table 1 lists the resulting 11 CIRs and 13 CMEs used in the study. Storms are assigned identifiers starting with an "I" or "M" for those with CIR or CME storm drivers, respectively, and are numbered in order of increasing strength (as defined by minimum *Dst**).

2.4. Comprehensive Ring Current Model

[16] The CRCM evaluates ring current particle distributions by solving the bounce-averaged Boltzmann equation self-consistently with a calculated ionospheric electric field (Rice Convection Model or RCM) [*Fok et al*., 2001]. It uses solar wind data (flow speed, density, and magnetic field), activity indices (Ap, Kp, *Dst*, and F10.7 flux), and initial populations of H^+, O^+, and electrons as input parameters. The model includes most of the significant ring current gain and loss processes: convective drift inward through the nightside and outward through the dayside, charge exchange with the neutral atmosphere, particle losses into the atmosphere, magnetopause shadowing, and diffusion by magnetic and electric field fluctuations. For this study, however, it does not include losses due to Coulomb interactions (drag or pitch angle scattering) or wave-particle interactions (pitch angle scattering).

[17] For this study, the CRCM is configured to model H^+ and O^+ distributions using the T96 magnetic field model [*Tsyganenko and Stern*, 1996], the Weimer high-latitude potential model [*Weimer*, 2001], the Tsyganenko-Mukai boundary model [*Tsyganenko and Mukai*, 2003] for ion temperature and density at 10 R_E (with an assumed Maxwellian distribution), an O^+/H^+ ratio from *Young et al*. [1982], and an L-shell [*McIlwain*, 1961] range of 2 to 10. The model is started 12 h prior to storm start to reduce the effect of initial model instabilities.

[18] The Tsyganenko-Mukai empirical boundary model reflects steady state conditions for values of IMF B_z and solar wind speed and density and thus responds immediately to changes in solar wind conditions. The actual magnetosphere, however, does not respond immediately, so a delay of 3 h is introduced in the solar wind parameter values for input to the magnetic field model. The 3 h value corresponds to a value midway between the time lag values determined by *Borovsky et al*. [1998] for the mid-tail plasma sheet and

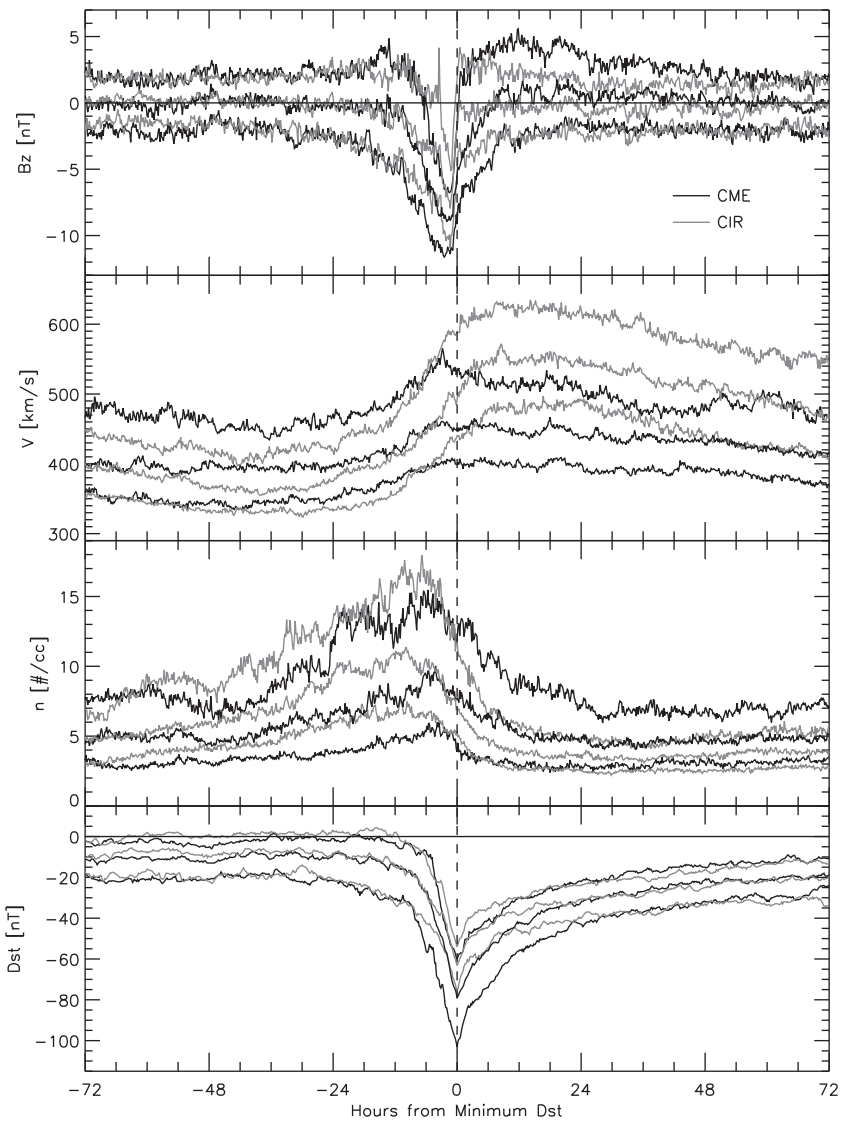

Figure 1. Superposed epoch analysis of solar wind profiles during storms with minimum $Dst^* \geq -120$ nT driven by CMEs (solid black lines) and CIRs (solid gray lines) between the years 1996 and 2006. The panels show, from top to bottom, the IMF north-south component (B_z), the solar wind velocity (V) and density (n), and *Dst*. The three lines represent the upper quartile, the median, and the lower quartile (from top to bottom). The vertical dashed line corresponds to the time of storm peak (minimum *Dst*).

geosynchronous orbit at midnight local time. To verify that this method improves the reproduction of *Dst**, the CRCM was run for five cases: a 0, 1, 2, 3, and 4 h delay. The 3 h delay was found to more frequently result in the best reproduction of the shape of *Dst** and time of minimum *Dst**. However, there are a few cases where shorter delays resulted in better simulated *Dst** for the initial rapid decrease in the main phase (e.g., I7 and M10).

[19] The CRCM initial particle population is set to match that of the quiet-time ring current, as derived by *Fok et al.* [1996] from AMPTE/CCE/CHEM data and compiled by *Sheldon and Hamilton* [1993]. In order to match the CRCM ΔB to actual *Dst** at the time of model start, the CRCM initial quiet values are reduced to the necessary level for each storm by multiplying all quiet-time flux values by a percentage (Table 1).

[20] Inconsistencies between the separate boundary condition calculations and the magnetic field model calculations have been found to be problematic in attempts to recreate *Dst** with the CRCM. To avoid this problem, a static magnetic field configuration based on peak conditions is used throughout the run. Input parameters to the magnetic field model (P_{dyn}, *Dst*, B_y, and B_z) were calculated by averaging values within 12 h of the storm peak (time of minimum *Dst**). Of the two models that are available in this version of the CRCM, the T96 model was chosen over the TS05 model [*Tsyganenko and Sitnov*, 2005] due to the difficulty in determining average conditions for the required integral inputs for the latter. This configuration was found to generate much better results than using a time-varying magnetic field. It is recognized that this does not represent reality and that significant ring current processes are left

Table 1. List of Modeled Storms

ID	Driver	Start Date	Minimum *Dst** [nT]	Initial Quiet (%)
I1	CIR	9 September 2003	–38	1
I2	CIR	6 June 1998	–44	30
I3	CIR	10 March 1996	–58	30
I4	CIR	11 January 2000	–68	50
I5	CIR	4 April 2005	–74	50
I6	CIR	13 October 2003	–82	10
I7	CIR	27 February 1997	–86	90
I8	CIR	10 July 2003	–92	1
I9	CIR	10 March 1998	–105	10
I10	CIR	20 November 2002	–114	100
I11	CIR	7 May 2005	–126	1
M1	CME	10 August 2005	–45	40
M2	CME	22 August 1995	–53	1
M3	CME	31 October 2005	–65	40
M4	CME	17 May 2000	–90	100
M5	CME	15 May 1997	–98	1
M6	CME	28 October 2000	–102	40
M7	CME	11 February 2000	–127	40
M8	CME	28 October 2001	–136	70
M9	CME	25 September 1998	–177	100
M10	CME	24 August 2005	–217	30
M11	CME	21 October 1999	–233	1
M12	CME	6 April 2000	–270	100
M13	CME	20 November 2003	–366	80

un-modeled, such as particle energization and transport due to magnetospheric compression and fluctuating fields. However, steady convection and flow-out losses, as well as other previously mentioned loss processes, are modeled.

3. Model Results

3.1. Individual Storms

[21] Table 1 lists all of the storms modeled by the CRCM for this study. Figure 2 shows *Dst** and resultant CRCM ΔB for each storm. In general, the shape of the model ΔB and *Dst** curves for each storm in Figure 2 are similar. The times of minimum ΔB and *Dst** also correspond well.

[22] However, the magnitude of *Dst** is underpredicted for a number of storms. Four of the underpredicted storms (M9, M11, M12, and M13) have T96 magnetic field input parameters that are truncated because they are outside of the allowed limits (storm peak ± 12 h-averaged $Dst \geq -100$ nT, and B_y and B_z within ± 10 nT), which is believed to be the cause of the underprediction. The *Dst** is also significantly underpredicted by the model for most of the stronger CIR-driven storms (e.g., I7, I8, I9, and I11).

[23] The *Dst** of the 28 October 2001, CME-driven storm (M8) is also underpredicted, displaying the worst agreement between modeled and actual *Dst** of any of the storms in this study (those that do not exceed T96 limits). This particular storm has a few features that are different from the other CME-driven storms in this study. First of all, there are larger fluctuations in B_z during this storm than the other storms in the study, or typical CME-driven storms in general. The associated rapid increase in solar wind velocity is also similar to that of high-speed streams (HSS). Perhaps most importantly, there is a rapid fivefold increase in solar wind dynamic pressure at the start of the main phase (Figure 3). Within a few minutes, the dynamic pressure increases from a very low value of less than 1.0 nPa to greater than 5.0 nPa. This quickly compresses the magnetosphere, which has been shown to energize the ring current [*Lee et al.*, 2007]. This energization mechanism is not captured by the CRCM in this study due to the fixed magnetic field.

[24] Other instances of poor agreement between model ΔB and *Dst** are found to occur during periods when the IMF is directed northward (B_z is positive). Normally, northward-directed IMF has the effect of shutting off convection into the inner magnetosphere, allowing the ring current energy to decrease (recover) through normal loss processes. However, in the pre-storm or early main phases of a few storms where B_z is positive or barely negative (e.g., I4, M1, M3, and M6), the model holds the ring current energy steady instead.

3.2. Storm Strength and Driver Dependence

[25] Figure 4 shows CRCM ΔB as a function of *Dst** at the time of storm peak, as defined by time of minimum *Dst**, for each storm in Table 1. A range of 3 h before or after minimum *Dst** is used for selection of peak CRCM ΔB to account for any slight timing differences that may exist between the model ΔB and *Dst**. The four CMEs with T96 magnetic field input parameters that are outside of the model limits (M9, M11, M12, and M13) are excluded. The 28 October 2001 storm (M8) is also excluded because adiabatic energization of the ring current due to magnetosphere compression appears to play a significant role that is not captured by the CRCM due to the fixed magnetic field. The remaining CME storm results have very good agreement between CRCM ΔB and *Dst**. The CIR results, however, are much less consistent.

[26] The lines on Figure 4 represent least-squares linear fits to the results (dotted line: CMEs; solid line: CIRs). The correlation coefficients are 0.99 and 0.59 for CME and CIR values, respectively. There appears to be a difference

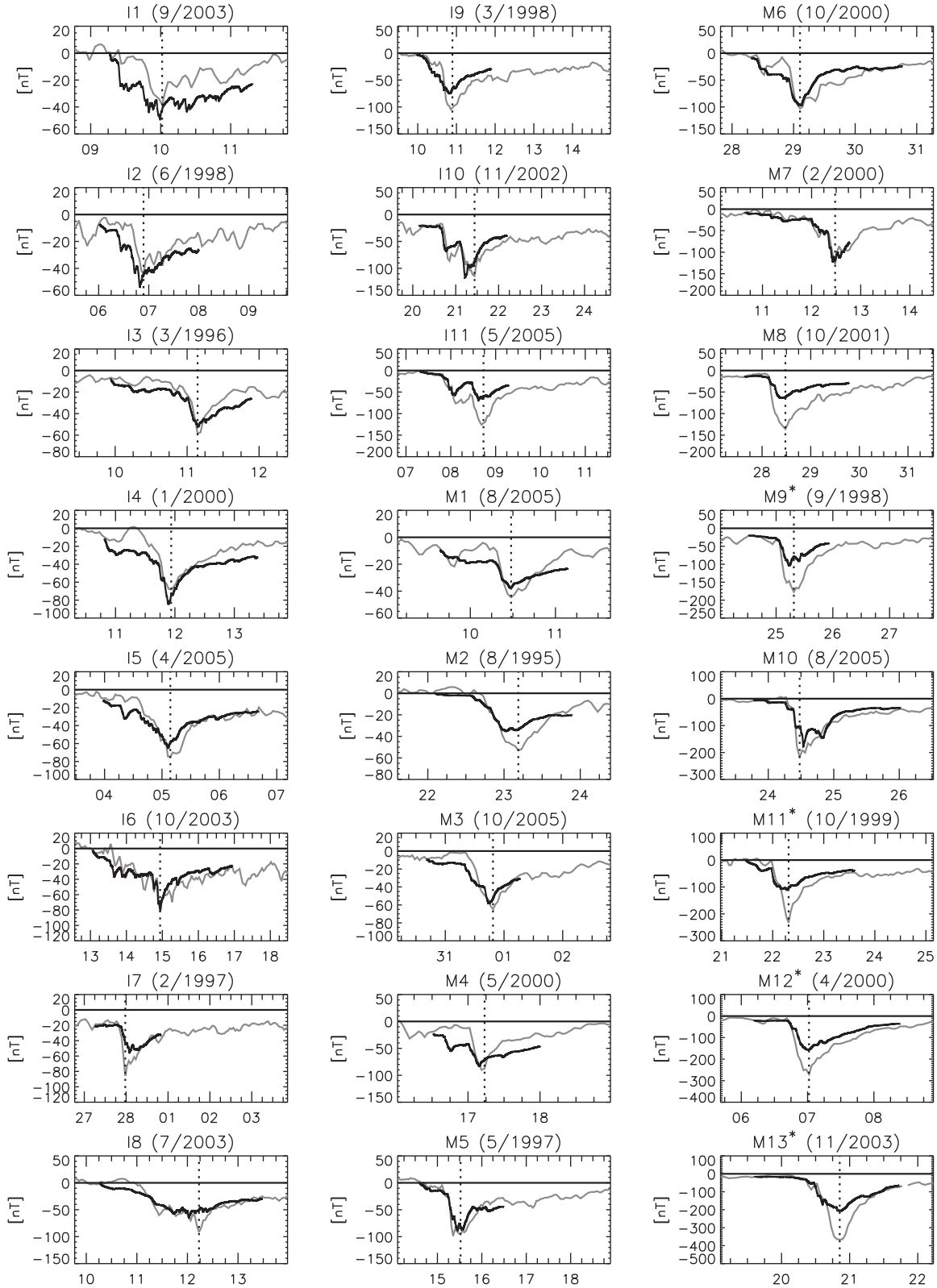

Figure 2. *Dst** (solid gray lines) and CRCM-derived ΔB (solid black lines) for the storms in this study. Storm identifiers start with an "I" or "M" for those with CIR or CME storm drivers, respectively, and are numbered in order of increasing strength. Storms with identifiers marked with an asterisk had T96 magnetic field model input parameters that were truncated to fall within model limits.

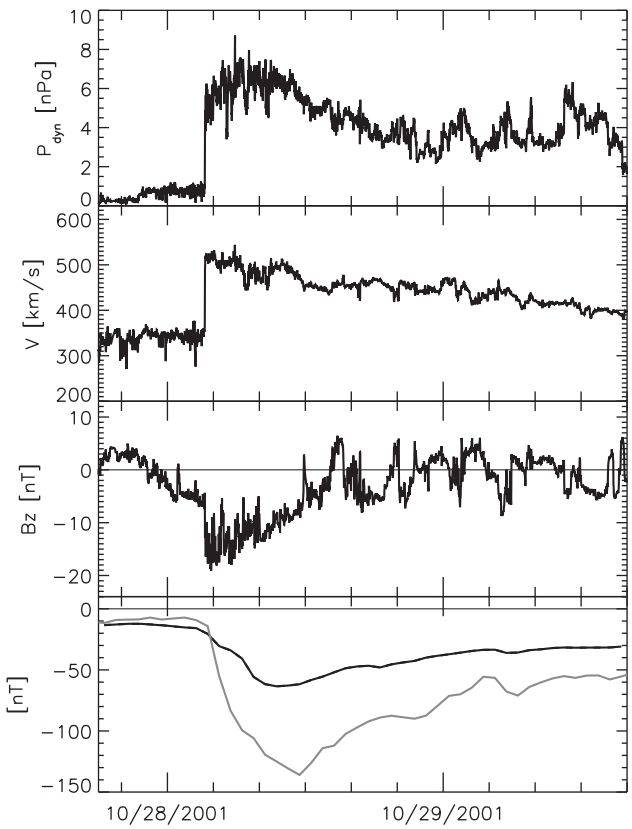

Figure 3. (From top to bottom) Solar wind dynamic pressure, solar wind velocity, north-south component of the IMF, and CRCM ΔB (black line) and *Dst** (gray line) during the CME-driven storm of 28 October 2001 (M8).

in the dependence of CRCM ΔB on *Dst** at storm peak for storms driven by CIRs and CMEs. While there is good agreement, in general, for CME-driven storms, weak CIR-driven storms appear to be overpredicted while stronger ones appear to be underpredicted. To test whether sub-storm energization of the ring current can explain the discrepancy in modeled and actual *Dst**, the AE index prior to storm peak is compared to the ratio of CRCM ΔB to *Dst** (Figure 5). For the modeled CIR-driven storms, the trend is such that modeled *Dst** for storms with stronger sub-storm activity (higher average AE) is underpredicted, while modeled *Dst** for storms with weaker sub-storm activity (lower average AE) is overpredicted. This indicates that model underprediction of *Dst** could be due to the failure to take sub-storm energization into account. However, regression analysis does not show that dependence of the ratio on AE is statistically significant (p-value = 0.15 that the slope of the line is zero).

[27] The relationship between ΔB and *Dst** for both sets of storms appears to be approximately linear, so regression analysis is used to determine if the best fit lines for CME and CIR-driven storms are different. The regression model defined by equation (3) is selected such that CME-driven storms have the model (4) and CIR-driven storms the model (5), where *Driver* equals 1 for CIR-driven and 0 for CME-driven storms. An analysis of variance test rejects the hypothesis that $\beta_2 = \beta_3 = 0$ (p-value = 0.0090), which shows that there is a significant difference in the line fits.

$$CRCM\ \Delta B = \beta_0 + \beta_1 \left(Dst^*_{\min}\right) + \beta_2(Driver) + \beta_3 \left(Dst^*_{\min}\right)(Driver) \tag{3}$$

$$(CRCM\ \Delta B)_{\mathrm{cme}} = \beta_0 + \beta_1 \left(Dst^*_{\min}\right) \tag{4}$$

$$(CRCM\ \Delta B)_{\mathrm{cir}} = (\beta_0 + \beta_2) + (\beta_1 + \beta_3) \left(Dst^*_{\min}\right) \tag{5}$$

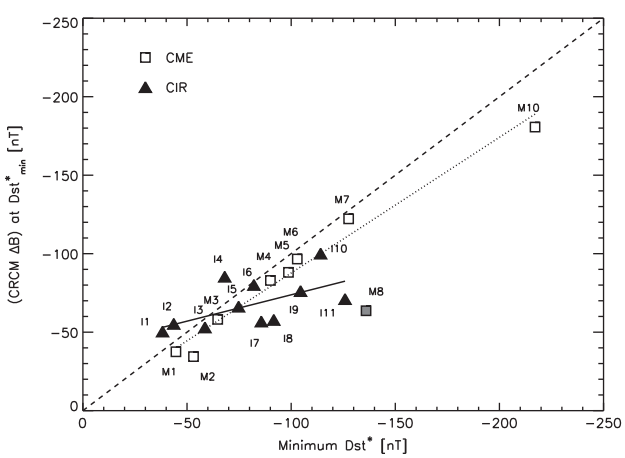

Figure 4. *Total ring current*. Minimum CRCM ΔB within 3 h of minimum *Dst**, as a function of minimum *Dst**. Storms driven by CMEs are represented as squares and those driven by CIRs by filled triangles. Storm strength, as measured by minimum *Dst**, increases from left to right. The dashed line represents a slope of unity. The dotted and solid lines are best fit lines to CME (all except M8) and CIR results, respectively.

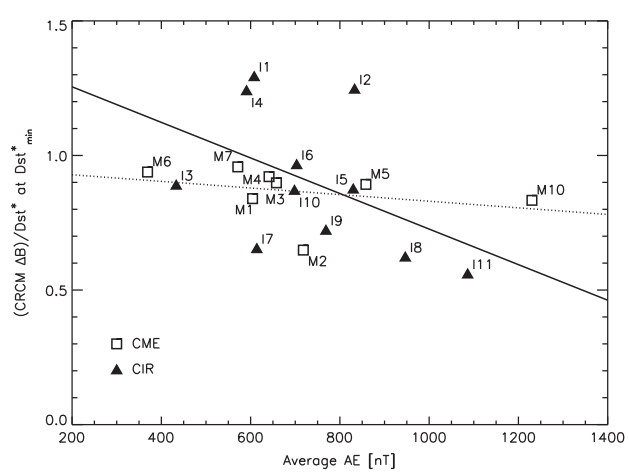

Figure 5. Ratio of Minimum CRCM ΔB within 3 h of minimum *Dst** to minimum *Dst**, as a function of average AE index during the 6 h prior to storm peak (minimum *Dst**). Storms driven by CMEs are represented as squares and those driven by CIRs by filled triangles. The dotted and solid lines are best fit lines to CME and CIR results, respectively.

3.3. Comparison to Previous Results

[28] *Liemohn and Jazowski* [2008] and, later, *Liemohn et al*. [2010] used the HEIDI model to simulate 79 storms (11 of which were CIR-driven). These storms were taken from the database compiled by *Zhang et al*. [2007a, 2007b] of storms between 1996 and 2005 that had a minimum $Dst \leq -100$ nT. They calculated a ratio of minimum DPS-derived *Dst** to minimum *Dst** for each storm, instead of using DPS-derived *Dst** at minimum *Dst** as in our study. *Liemohn et al*. [2010] modeled each storm, where possible, using five different combinations of plasma and electric field boundary conditions. In their study, the five-run-average ratios were 0.70 and 0.52 for CME and CIR-driven storms, respectively, meaning that CIR-driven storms underpredicted *Dst** by approximately 25% more than CME-driven storms.

[29] Figure 6 shows our results in a format comparable to *Liemohn and Jazowski* [2008] and *Liemohn et al*. [2010], using their definition of *Dst** (defined by equation (1) with the values of *a*, *b*, and *c* given as 1.3, 8.7, and 11.0, respectively), which will be hereafter referred to as Dst_L^*. The filled symbols represent storms that were too weak to be included in their studies. Storms with parameters beyond the limits of the T96 model (M9, M11, M12, and M13) are not included. Our results show that for the stronger storms, the average ratio of ΔB to Dst_L^* is 1.00 and 0.83 for CME and CIR-driven storms, respectively. This agrees with *Liemohn et al*. [2010] in that storms with a minimum $Dst \leq -100$ nT yielded lower average ratios for CIR-driven storms than CME-driven storms. However, in our study, ratios for the CIR-driven storms with a minimum $Dst > -100$ nT exceeded those of CME-driven storms (1.12 and 0.91, respectively). This implies that the observed underprediction of *Dst** for CIR-driven storms may only apply to stronger storms.

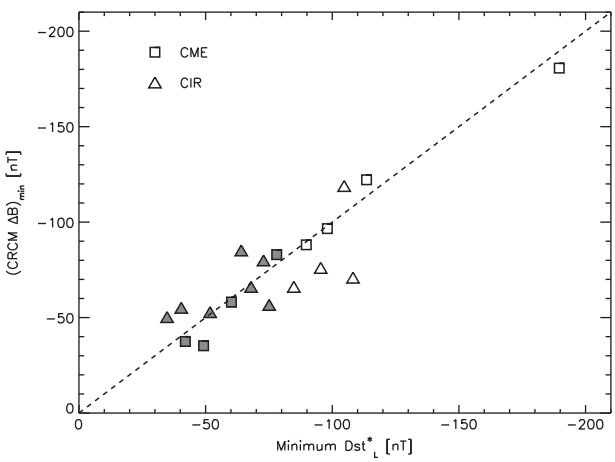

Figure 6. Minimum CRCM ΔB as a function of minimum Dst_L^*. Storms driven by CMEs are represented as squares and those driven by CIRs by triangles. Storm strength, as measured by minimum Dst_L^*, increases from left to right. The line represents a slope of unity. Filled symbols represent storms whose minimum *Dst* is greater than –100 nT.

[30] Figure 7 shows our results for the three storms highlighted by *Liemohn and Jazowski* [2008]. The Dst_L^* is underpredicted for the strongest CME-driven storm (March–April 2001). This can be explained by the fact that the T96 model inputs were beyond the magnetic field model limits for this storm. As for the other two storms, our study accurately predicts the Dst_L^* for the CME-driven storm (May 1997; M5) but underpredicts the CIR-driven storm (May 2005; I11). This is in agreement with *Liemohn and Jazowski* [2008], who showed a good match between actual and modeled Dst_L^* for the CME and underprediction for the CIR (Figures 1, 3, and 5 of that paper).

[31] Our results for individual storms seem to generally agree with those of the previous studies. However, we find that the ratio of ΔB to Dst_L^* is higher for CIR-driven storms than CME-driven ones for storms that were too weak to be included in those previous studies.

[32] Both *Jordanova* [2006] and *Jordanova et al*. [2009] modeled CME- and CIR-driven storms using the RAM model. *Jordanova* [2006] found that modeled SYM-H (an index that is similar to 1 min resolution *Dst*) was underestimated when compared to actual SYM-H during a CIR-driven storm (10 March 1998; I9) but was a good match during a CME-driven storm (15 May 1997; M5) [*Jordanova*, 2006, Figure 1]. *Jordanova et al*. [2009] showed similar results with two other storms: one CIR driven (23 October 2002) and one CME driven (22 April 2001). This led them to the conclusion that models underestimate the ring current for CIR-driven storms.

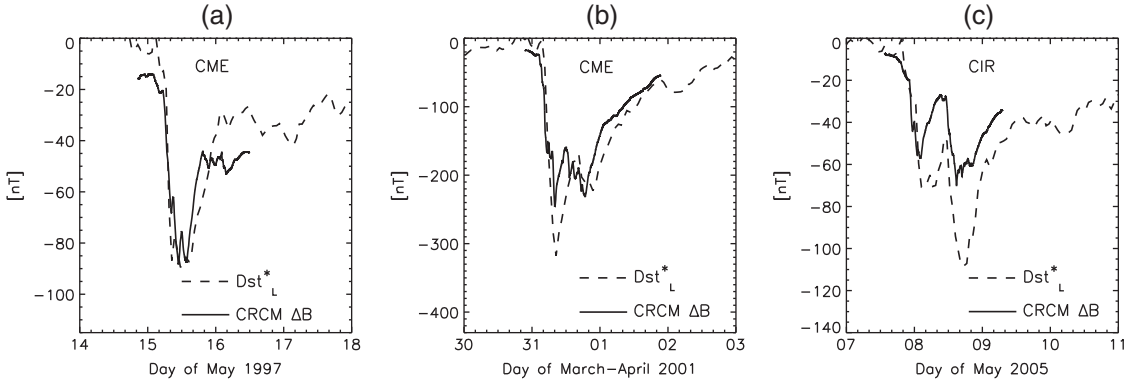

Figure 7. CRCM ΔB compared to Dst_L^* for two CME-driven storms, (a) and (b), and one CIR-driven storm, (c). The solid and dashed lines represent ΔB and Dst_L^*, respectively.

[33] For our comparison, we modeled the same four events. Figure 8 shows actual and modeled *Dst** for these storms. For the storms modeled by *Jordanova* [2006], we compared to the results calculated with the Weimer 2001 potential model [*Weimer*, 2001] and no radial diffusion (Figure 1 of that paper). For the storms modeled by *Jordanova et al*. [2009] (Figure 4 of that paper), we compared to the results calculated with the Volland-Stern potential model [*Volland*, 1973; *Stern*, 1975; *Maynard and Chen*, 1975]. Our minimum modeled *Dst** values for the CIR-driven storms were within 10 nT of theirs; however, our values for the CME-driven storms had magnitudes that were much lower (a greater than 20 nT difference). The model minimum *Dst** for the May 1997 CME-driven storm was the closest to the actual minimum *Dst** (11% underpredicted), while the April 2001 CME-driven storm had the worst agreement (47% underpredicted, resulting in an average of 29% for the two storms). It is not clear what is causing the severe underprediction in the latter case, as no unusual behavior was noted in solar wind data or the AE index. Both CIR-driven storms were underpredicted by approximately 29%, so we do not find a dependence in underprediction on storm driver. The main difference between our results and those of the previous studies is the lower magnitude of modeled *Dst** of our CME-driven storm results.

[34] Our CRCM study has an advantage over these other studies in that its computational domain (up to L-shell of 10) includes the entirety of the ring current. By contrast, the outer boundaries of the HEIDI and RAM models were L-shells of 6.6 and 6.5, respectively. Figure 9 shows the ratio of ΔB for the total ring current energy to inner ring current energy (within an L-shell of 6.6) at the storm peak for the storms in this study. On average, about half of the total ring current energy lies between L-shells of 6.6 and 10 (approximately 50% and 42% for the CME- and CIR-driven storms, respectively). However, the use of a static magnetic field in the CRCM likely overestimates this value by limiting radial transport and, therefore, depth of particle penetration. Regardless, the ring current region beyond geosynchronous orbit can contribute a significant amount to the total ring current energy, even when it contains low energy densities, due to large flux tube volumes.

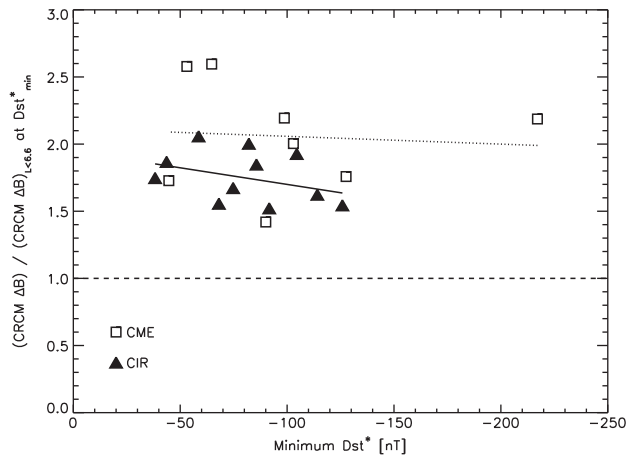

Figure 9. Ratio of CRCM ΔB to CRCM ΔB within a boundary at L-shell of 6.6, as a function of minimum *Dst**, plus or minus 3 h. Storms driven by CMEs are represented as squares and those driven by CIRs by filled triangles. Storm strength, as measured by minimum *Dst**, increases from left to right. The dotted and solid lines are best fit lines to CME (all except M8) and CIR results, respectively.

4. Discussion

4.1. CRCM Reproduction of Dst*

[35] The configuration of the CRCM used for this study predicts peak storm *Dst** for CME-driven storms very well, when the associated solar wind parameters are within model limits. The sole exception in our study is the 28 October 2001 storm (M8), which is significantly underpredicted. The predicted peak *Dst** values for CIR-driven storms, on the other hand, show large deviations. The weaker CIR-driven storms (*Dst** below approximately –55 nT) are overpredicted, while stronger ones are underpredicted. In fact, for storms with this driver, agreement with minimum *Dst** appears to get worse as storm strength increases.

[36] After testing with a variety of model settings, we are confident that those chosen are close to optimal for reproducing *Dst**. However, the determination of time delay between solar wind conditions and plasma sheet density

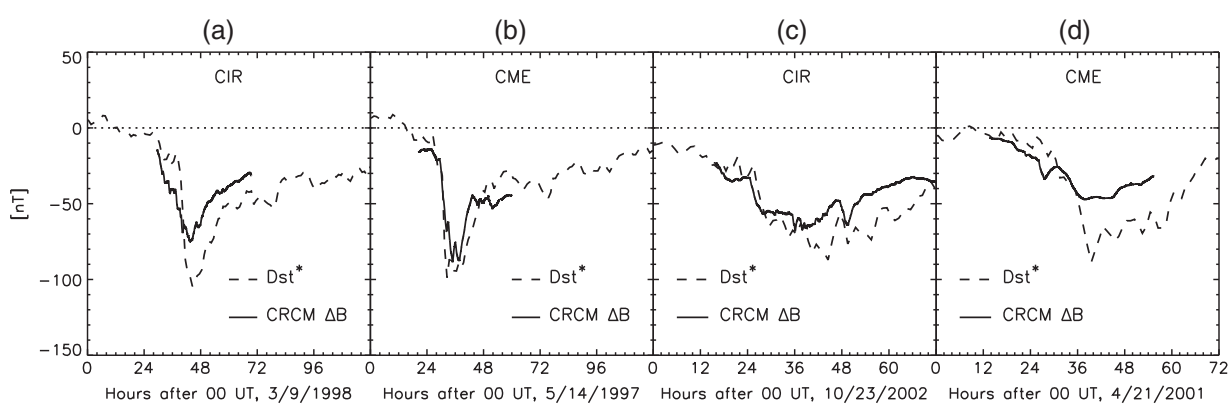

Figure 8. CRCM ΔB compared to *Dst** for two CIR-driven storms, (a) and (c), and two CME-driven storms, (b) and (d). The solid and dashed lines represent ΔB and *Dst**, respectively.

appears to have the potential for improvement. For this study, we use a 3 h delay between solar wind changes and plasma sheet density calculations. Although this results in better agreement with times of minimum *Dst** and overall shape of *Dst**, removing the delay sometimes results in better agreement with initial, rapid *Dst** drops in the main phase. This hints at the possibility that the plasma sheet may respond rapidly to solar wind conditions that drive an increase in density, while responding much slower to those that would lower it.

[37] Because we are holding the magnetic field constant, our model setup can only evaluate the effects of convection and boundary conditions on ring current energy content. Other mechanisms that affect the ring current, such as substorms and the effects of external currents, are obviously not included. The fact that these results reproduce the shape of *Dst** very well indicates that convection and boundary conditions are the main factors affecting *Dst**. Work is currently being done to couple MHD models to the CRCM in order to improve the model response by modeling magnetic field fluctuations self-consistently with the global dynamics of the magnetosphere [*Fok et al*., 2006; *Buzulukova et al*., 2010; *Fok et al*., 2011].

4.2. Dependence on Driver

[38] The agreement between CRCM ΔB and *Dst** is especially good for CME-driven storms, not just in shape but in minimum *Dst**, which seems to show that factors other than convection and boundary conditions are minor for these storms. The results for CIR-driven storms, on the other hand, have larger deviations from actual *Dst**. Other mechanisms appear to be more important for this class of storms, although our study does not clearly identify which ones. One possible explanation is that the large, rapid oscillations in solar wind parameters due to Alfvén waves that are associated with CIR-driven storms contribute to ring current energization through some non-convective mechanism. In particular, these waves have previously been shown to drive sub-storm activity. Our analysis seems to show a relationship between sub-storm activity and agreement between modeled and actual *Dst** for CIR-driven storms (Figure 5). However, we could not show that statistically.

[39] We find that CRCM ΔB dependence on *Dst** at storm peak is significantly different for CMEs and CIRs. This was determined by using a regression model with driver-dependent parameters and showing that they significantly differed from a value of zero.

[40] The model greatly underestimated *Dst** for the 28 October 2001 storm (M8). Adiabatic energization due to rapid magnetosphere compression appears to explain the unexpectedly large *Dst** response. The CRCM is set up to only model the effects of convection and therefore does not account for this additional mechanism. This particular storm also has solar wind features commonly associated with CIRs, such as large oscillations in B_z and a rapid increase in solar wind velocity, which could also contribute to the different *Dst** response.

4.3. Comparison to Previous Research

[41] Our results have good agreement with those of *Liemohn and Jazowski* [2008], *Liemohn et al*. [2010], and *Jordanova* [2006], in that CIR-driven storms tend to be more underpredicted by models, but only when stronger storms are considered. However, our results with the two storms modeled by *Jordanova et al*. [2009] seemed to show the opposite, due to a 47% underprediction of *Dst** by the CRCM in the case of the CME-driven storm. It was also noted that very weak CIR-driven storms were actually overpredicted.

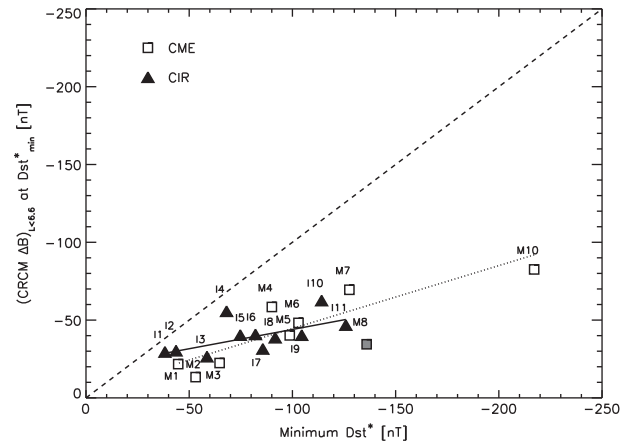

Figure 10. *Inner ring current.* Minimum CRCM ΔB within 3 h of minimum *Dst**, calculated within a boundary at L-shell of 6.6, as a function of minimum *Dst**. Storms driven by CMEs are represented as squares and those driven by CIRs by filled triangles. Storm strength, as measured by minimum *Dst**, increases from left to right. The dashed line represents a slope of unity. The dotted and solid lines are best fit lines to CME (all except M8) and CIR results, respectively.

[42] The expanded boundary of the CRCM in our study (out to an L-shell of 10) has the advantage of including the entire ring current domain. The improvement in the results is evident, especially for CME-driven storms, when comparing Figure 4 to Figure 10, which only includes ring current energy within an L-shell boundary of 6.6.

5. Conclusions

[43] We used the CRCM to model 13 CME-driven and 11 CIR-driven storms. Each storm that was selected had solar wind parameters that fit a typical profile for storms caused by its particular solar wind driver. Surface equatorial magnetic disturbance was estimated from the modeled ring current energy and compared to *Dst** at storm peak. Our results show the following:

[44] 1. With our configuration, the CRCM predicts the shape of *Dst** well and, in the case of CME-driven storms, the minimum *Dst** very well. Given the processes modeled with the CRCM, this indicates that convection and plasma sheet density at the boundary are the most important factors controlling *Dst** for these types of storms. However, there is substantial variation between actual and simulated *Dst** for CIR-driven storms. Sub-storm activity appears to play a role in ring current energization for these types of storms.

[45] 2. There are limitations on the strength of storms that can be modeled by the CRCM, as configured for this

study, due to the limitations of the T96 magnetic field model. The relationship between solar wind conditions and plasma sheet density at the model boundary also appears to be more complicated than can be simulated by a simple time delay.

[46] 3. Our results find a significant difference between CIR- and CME-driven ring current modeled *Dst** when compared to *Dst** for storms of similar strength.

[47] 4. When comparing our individual storm results to previous studies, we generally agree that *Dst** for CIR-driven storms is more underpredicted than for that of CME-driven storms, but only for stronger CIR-driven storms (minimum $Dst^* \leq -50$ nT). We find that weaker CIR-driven storms are actually overpredicted.

[48] 5. We find that approximately half of the total ring current energy lies beyond an L-shell of 6.6 (50% and 42% for CME and CIR-driven storms, respectively). The CRCM domain encompasses the entire ring current region, so it has the advantage over other models of including outer ring current effects. However, the use of a static magnetic field in the CRCM may limit radial transport into the inner ring current, causing overestimation of the energy content of the outer region.

[49] **Acknowledgments.** This research was funded though the NASA Graduate Student Researchers Program Fellowship (Grant No. NNX08AT39H) and the NSF Career Program (Grant No. 0454685). We thank Hohlmann from the Florida Tech High Energy Physics group and for use of their computing cluster, Haje Korth for the use of his IDL Geopack DLM for the Tsyganenko model, and NOAA for their weekly space weather reports, and we acknowledge the use of the OMNI solar wind database through CDAWeb. This material is based upon work supported by the NSF under Grant No. 09-23050. We also thank Ismael Diaz and Cameo for their helpful comments.

References

Baker, D. N., and I. A. Daglis (2006), Radiation belts and ring current, in *Space Weather—Physics and Effects*, chap. 6, Springer Verlag, Berlin, 173–202.

Baker, D. N., N. E. Turner, and T. I. Pulkkinen (2001), Energy transport and dissipation in the magnetosphere during geomagnetic storms, *J. Atmos. Sol. Terr. Phys.*, *63*, 421–429, doi:10.1016/S1364-6826(00)00169-3.

Borovsky, J. E., M. F. Thomsen, and R. C. Elphic (1998), The driving of the plasma sheet by the solar wind, *J. Geophys. Res.*, *103*, 17,617–17,640, doi:10.1029/97JA02986.

Burke, W. J., L. C. Gentile, and M. P. Hagan (2010), Thermospheric heating by high-speed streams in the solar wind, *J. Geophys. Res.*, *115*, A06318, doi:10.1029/2009JA014585.

Burton, R. K., R. L. McPherron, and C. T. Russell (1975), An empirical relationship between interplanetary conditions and Dst, *J. Geophys. Res.*, *80*, 4204–4214, doi:10.1029/JA080i031p04204.

Buzulukova, N., M.-C. Fok, A. Pulkkinen, M. Kuznetsova, T. E. Moore, A. Glocer, P. C. Brandt, G. Tóth, and L. Rastätter (2010), Dynamics of ring current and electric fields in the inner magnetosphere during disturbed periods: CRCM-BATS-R-US coupled model, *J. Geophys. Res.*, *115*, A05210, doi:10.1029/2009JA014621.

Campbell, W. H. (1996), Geomagnetic storms, the Dst ring-current myth and lognormal distributions, *J. Atmos. Terr. Phys.*, *58*(10), 1171–1187.

Cane, H. V., and I. G. Richardson (2003), Interplanetary coronal mass ejections in the near-Earth solar wind during 1996–2002, *J. Geophys. Res.*, *108*, 1156, doi:10.1029/2002JA009817.

Chen, M. W., M. Schulz, and L. R. Lyons (1997), Modeling of ring current formation and decay: A review, in *Magnetic Storms, Geophys. Monogr. Ser.*, edited by Tsurutani, B. T., W. D. Gonzalez, Y. Kamide, and J. K. Arballo, vol. 98, AGU, Washington, D. C., 173–186.

Daglis, I. A. (2006), Ring current dynamics, *Space Sci. Rev.*, *124*, 183–202, doi:10.1007/s11214-006-9104-z.

Denton, M. H., and J. E. Borovsky (2009), The superdense plasma sheet in the magnetosphere during high-speed-stream-driven storms: Plasma transport timescales, *J. Atmos. Sol. Terr. Phys.*, *71*, 1045–1058, doi: 10.1016/j.jastp.2008.04.023.

Dessler, A. J., and E. N. Parker (1959), Hydromagnetic theory of geomagnetic storms, *J. Geophys. Res.*, *64* (12), 2239–2252, doi: 10.1029/JZ064i012p02239.

Dungey, J. W. (1961), Interplanetary magnetic field and the auroral zones, *Phys. Rev. Lett.*, *6*, 47–48, doi:10.1103/PhysRevLett.6.47.

Fenrich, F. R., and J. G. Luhmann (1998), Geomagnetic response to magnetic clouds of different polarity, *Geophys. Res. Lett.*, *25*(15), 2999–3002, doi:10.1029/98GL51180.

Fok, M.-C., J. U. Kozyra, A. F. Nagy, and T. E. Cravens (1991), Lifetime of ring current particles due to Coulomb collisions in the plasmasphere, *J. Geophys. Res.*, *96*, 7861–7867, doi:10.1029/90JA02620.

Fok, M.-C., T. E. Moore, and M. E. Greenspan (1996), Ring current development during storm main phase, *J. Geophys. Res.*, *101*, 15,311–15,322, doi:10.1029/96JA01274.

Fok, M.-C., R. A. Wolf, R. W. Spiro, and T. E. Moore (2001), Comprehensive computational model of Earth's ring current, *J. Geophys. Res.*, *106*, 8417–8424, doi:10.1029/2000JA000235.

Fok, M.-C., Y. Ebihara, and T. E. Moore (2005), Inner magnetospheric plasma interactions and coupling with the ionosphere, *Adv. Polar Upper Atmos. Res.*, *19*, 106–134.

Fok, M.-C., T. E. Moore, P. C. Brandt, D. C. Delcourt, S. P. Slinker, and J. A. Fedder (2006), Impulsive enhancements of oxygen ions during substorms, *J. Geophys. Res.*, *111*, A10222, doi:10.1029/2006JA011839.

Fok, M.-C., T. E. Moore, S. P. Slinker, J. A. Fedder, D. C. Delcourt, M. Nosé, and S.-H. Chen (2011), Modeling the superstorm in November 2003, *J. Geophys. Res.*, *116*, A00J17, doi:10.1029/2010JA015720.

Fritz, T. A. (2001), The cusp as a source of magnetospheric energetic particles, currents, and electric fields: A new paradigm, *Space Sci. Rev.*, *95*, 469–488.

Ganushkina, N., T. Pulkkinen, M. Kubyshkina, H. Singer, and C. Russell (2004), Long-term evolution of magnetospheric current systems during storms, *Ann. Geophys.*, *22*, 1317–1334, doi:10.5194/angeo-22-1317-2004.

Ganushkina, N. Y., T. I. Pulkkinen, V. A. Sergeev, M. V. Kubyshkina, D. N. Baker, N. E. Turner, M. Grande, B. Kellett, J. Fennell, J. Roeder, J.-A. Sauvaud, and T. A. Fritz (2000), Entry of plasma sheet particles into the inner magnetosphere as observed by Polar/CAMMICE, *J. Geophys. Res.*, *105*, 25,205–25,220, doi:10.1029/2000JA900062.

Häkkinen, L. V. T., T. I. Pulkkinen, H. Nevanlinna, R. J. Pirjola, and E. I. Tanskanen (2002), Effects of induced currents on Dst and on magnetic variations at midlatitude stations, *J. Geophys. Res.*, *107*, 1014, doi: 10.1029/2001JA900130.

Häkkinen, L. V. T., T. I. Pulkkinen, R. J. Pirjola, H. Nevanlinna, E. I. Tanskanen, and N. E. Turner (2003), Seasonal and diurnal variation of geomagnetic activity: Revised Dst versus external drivers, *J. Geophys. Res.*, *108*(A2), 1060, doi:10.1029/2002JA009428.

Jordanova, V. K. (2006), Modeling the behavior of corotating interaction region driven storms in comparison with coronal mass ejection driven storms, in *Recurrent Magnetic Storms: Corotating Solar Wind Streams,* vol. 167, *Geophys. Monogr. Ser.*, edited by Tsurutani, B. T., R. McPherron, W. Gonzalez, G. Lu, J. H. A. Sobral, and N. Gopalswamy, pp. 77–84, AGU, Washington, D. C.

Jordanova, V. K., L. M. Kistler, J. U. Kozyra, G. V. Khazanov, and A. F. Nagy (1996), Collisional losses of ring current ions, *J. Geophys. Res.*, *101*, 111–126, doi:10.1029/95JA02000.

Jordanova, V. K., J. U. Kozyra, A. F. Nagy, and G. V. Khazanov (1997), Kinetic model of the ring current-atmosphere interactions, *J. Geophys. Res.*, *1021*, 14,279–14,292, doi:10.1029/96JA03699.

Jordanova, V. K., H. Matsui, P. A. Puhl-Quinn, M. F. Thomsen, K. Mursula, and L. Holappa (2009), Ring current development during high speed streams, *J. Atmos. Sol. Terr. Phys.*, *71*, 1093–1102, doi:10.1016/j.jastp.2008.09.043.

Kozyra, J. U., and M. W. Liemohn (2003), Ring current energy input and decay, *Space Sci. Rev.*, *109*, 105–131, doi:10.1023/B:SPAC.0000007516.10433.ad.

Langel, R. A., and R. H. Estes (1985), Large-scale, near-field magnetic fields from external sources and the corresponding induced internal field, *J. Geophys. Res.*, *90*, 2487–2494, doi:10.1029/JB090iB03p02487.

Lee, D.-Y., S. Ohtani, P. C. Brandt, and L. R. Lyons (2007), Energetic neutral atom response to solar wind dynamic pressure enhancements, *J. Geophys. Res.*, *112*, A09210, doi:10.1029/2007JA012399.

Liemohn, M. W., and M. Jazowski (2008), Ring current simulations of the 90 intense storms during solar cycle 23, *J. Geophys. Res.*, *113*, A00A17, doi:10.1029/2008JA013466.

Liemohn, M. W., and R. Katus (2012), Is the storm time response of the inner magnetospheric hot ions universally similar or driver dependent?, *J. Geophys. Res.*, *117*, A00L03, doi:10.1029/2011JA017389.

Liemohn, M. W., M. Jazowski, J. U. Kozyra, N. Ganushkina, M. F. Thomsen, and J. E. Borovsky (2010), CIR versus CME drivers of the

ring current during intense magnetic storms, *Proc. R. Soc. A*, *466*, 3305–3328, doi:10.1098/rspa.2010.0075.

Lyons, L. R., and M. Schulz (1989), Access of energetic particles to storm time ring current through enhanced radial 'diffusion', *J. Geophys. Res.*, *94*, 5491–5496, doi:10.1029/JA094iA05p05491.

Maynard, N. C., and A. J. Chen (1975), Isolated cold plasma regions—Observations and their relation to possible production mechanisms, *J. Geophys. Res.*, *80*, 1009–1013, doi: 10.1029/JA080i007p01009.

McIlwain, C. E. (1961), Coordinates for mapping the distribution of magnetically trapped particles, *J. Geophys. Res.*, *66*, 3681–3691, doi: 10.1029/JZ066i011p03681.

O'Brien, T. P., and R. L. McPherron (2000), An empirical phase space analysis of ring current dynamics: Solar wind control of injection and decay, *J. Geophys. Res.*, *105*, 7707–7720, doi:10.1029/1998JA000437.

Ohtani, S., M. Nosé, G. Rostoker, H. Singer, A. T. Y. Lui, and M. Nakamura, (2001), Storm-substorm relationship: Contribution of the tail current to Dst, *J. Geophys. Res.*, *106*(A10), 21,199–21,210, doi: 10.1029/2000JA000400.

Pulkkinen, T. I., D. N. Baker, N. E. Turner, H. J. Singer, L. A. Frank, J. B. Sigwarth, J. Scudder, R. Anderson, S. Kokubun, R. Nakamura, T. Mukai, J. B. Blake, C. T. Russell, H. Kawano, F. Mozer, and J. A. Slavin (1997), Solar wind-magnetosphere coupling during an isolated substorm event: A multispacecraft ISTP study, *Geophys. Res. Lett.*, *24*, 983–986, doi: 10.1029/97GL00816.

Pulkkinen, T. I., N. Y. Ganushkina, D. N. Baker, N. E. Turner, J. F. Fennell, J. Roeder, T. A. Fritz, M. Grande, B. Kellett, and G. Kettmann (2001), Ring current ion composition during solar minimum and rising solar activity: Polar/CAMMICE/MICS results, *J. Geophys. Res.*, *106*, 19,131–19,148, doi:10.1029/2000JA003036.

Pulkkinen, T. I., N. Y. Ganushkina, E. I. Kallio, G. Lu, D. N. Baker, N. E. Turner, T. A. Fritz, J. F. Fennell, and J. Roeder (2002), Energy dissipation during a geomagnetic storm: May 1998, *Adv. Space Res.*, *30*, 2231–2240, doi:10.1016/S0273-1177(02)80232-0.

Sckopke, N. (1966), A general relation between the energy of trapped particles and the disturbance field near Earth, *J. Geophys. Res.*, *71*, 3125–3130.

Sheldon, R. B., and D. C. Hamilton (1993), Ion transport and loss in the Earth's quiet ring current. I—Data and standard model, *J. Geophys. Res.*, *98*, 13,491–13,508, doi:10.1029/92JA02869.

Stern, D. P. (1975), The motion of a proton in the equatorial magnetosphere, *J. Geophys. Res.*, *80*, 595–599, doi:10.1029/JA080i004p00595.

Tsurutani, B. T., and W. D. Gonzalez (1987), The cause of high-intensity long-duration continuous AE activity (HILDCAAS) - Interplanetary Alfven wave trains, *Planet. Space Sci.*, *35*, 405–412, doi:10.1016/0032-0633(87)90097-3.

Tsyganenko, N. A., and T. Mukai (2003), Tail plasma sheet models derived from Geotail particle data, *J. Geophys. Res.*, *108*, 1136, doi: 10.1029/2002JA009707.

Tsyganenko, N. A., and M. I. Sitnov (2005), Modeling the dynamics of the inner magnetosphere during strong geomagnetic storms, *J. Geophys. Res.*, *110*, A03208, doi:10.1029/2004JA010798.

Tsyganenko, N. A., and D. P. Stern (1996), Modeling the global magnetic field of the large-scale Birkeland current systems, *J. Geophys. Res.*, *101*, 27,187–27,198, doi:10.1029/96JA02735.

Turner, N. E. (2000), Solar wind-magnetosphere coupling and global energy budgets in the Earth's magnetosphere, Ph.D. thesis, University of Colorado.

Turner, N. E., D. N. Baker, T. I. Pulkkinen, and R. L. McPherron (2000), Evaluation of the tail current contribution to Dst, *J. Geophys. Res.*, *105* (A3), 5431–5440, doi:10.1029/1999JA000248.

Turner, N. E., D. N. Baker, T. I. Pulkkinen, J. L. Roeder, J. F. Fennell, and V. K. Jordanova (2001), Energy content in the storm time ring current, *J. Geophys. Res.*, *106*(A9), 19,149–19,156, doi:10.1029/2000JA003025.

Turner, N. E., T. I. Pulkkinen, D. N. Baker, and R. L. McPherron (2002), Reply to Comment on "Evaluation of the tail current contribution to Dst", *J. Geophys. Res.*, *107*, 1011, doi:10.1029/2001JA900099.

Turner, N. E., E. J. Mitchell, D. J. Knipp, and B. A. Emery (2006), Energetics of magnetic storms driven by corotating interaction regions: A study of geoeffectiveness, in *Recurrent Magnetic Storms: Corotating Solar Wind Streams,* vol. 167, *Geophys. Monogr. Ser.*, edited by Tsurutani, B. T., W. Gonzalez, G. Lu, J. H. A. Sobral, and N. Gopalswamy, pp. 113–124 AGU, Washington, D. C.

Turner, N. E., W. D. Cramer, S. K. Earles, and B. A. Emery (2009), Geoefficiency and energy partitioning in CIR-driven and CME-driven storms, *J. Atmos. Sol. Terr. Phys.*, *71*, 1023–1031, doi:10.1016/j.jastp.2009.02.005.

Volland, H. (1973), A semiempirical model of large-scale magnetospheric electric fields, *J. Geophys. Res.*, *78*, 171, doi:10.1029/JA078i001p00171.

Weimer, D. R. (2001), An improved model of ionospheric electric potentials including substorm perturbations and application to the Geospace Environment Modeling November 24, 1996, event, *J. Geophys. Res.*, *106*, 407–416, doi:10.1029/2000JA000604.

Young, D. T., H. Balsiger, and J. Geiss (1982), Correlations of magnetospheric ion composition with geomagnetic and solar activity, *J. Geophys. Res.*, *87*, 9077–9096, doi:10.1029/JA087iA11p09077.

Zhang, J., I. G. Richardson, D. F. Webb, N. Gopalswamy, E. Huttunen, J. Kasper, N. V. Nitta, W. Poomvises, B. J. Thompson, C. Wu, S. Yashiro, and A. N. Zhukov (2007a), Correction to "Solar and interplanetary sources of major geomagnetic storms (Dst $\leq$ –100 nT) during 1996–2005", *J. Geophys. Res.*, *112*, A12103, doi:10.1029/2007JA012891.

Zhang, J., I. G. Richardson, D. F. Webb, N. Gopalswamy, E. Huttunen, J. C. Kasper, N. V. Nitta, W. Poomvises, B. J. Thompson, C. Wu, S. Yashiro, and A. N. Zhukov (2007b), Solar and interplanetary sources of major geomagnetic storms (Dst $\leq$ –100 nT) during 1996–2005, *J. Geophys. Res.*, *112*, A10102, doi:10.1029/2007JA012321.